

- MOTHERWELL, W. D. S. (1974). *PLUTO*. Program for plotting molecular and crystal structures. Univ. of Cambridge, England.
- NARDELLI, M. (1983). *Comput. Chem.* **7**, 95–98.
- NASSIMBENI, L. R., NIVEN, M. L. & SUCKLING, A. P. (1989). *Inorg. Chim. Acta*, **159**, 209–217.
- NASSIMBENI, L. R., NIVEN, M. L. & TAYLOR, M. W. (1987). *Inorg. Chim. Acta*, **132**, 67–73.
- NASSIMBENI, L. R., NIVEN, M. L. & TAYLOR, M. W. (1989a). *J. Chem. Soc. Dalton Trans.* pp. 119–125.
- NASSIMBENI, L. R., NIVEN, M. L. & TAYLOR, M. W. (1989b). *J. Coord. Chem.* **19**, 339–348.
- NASSIMBENI, L. R., PAPANICOLAOU, S. & MOORE, M. H. (1986). *J. Inclusion Phenom.* **4**, 31–42.
- NORTH, A. C. T., PHILLIPS, D. C. & MATHEWS, F. S. (1968). *Acta Cryst.* **A24**, 351–359.
- RADZITZKY, P. DE & HANOTIER, J. (1962). *Ind. Eng. Chem. Process Des. Dev.* **1**, 10–14.
- SCHAEFFER, W. D., DORSEY, W. S., SKINNER, D. A. & CHRISTIAN, J. (1957). *J. Am. Chem. Soc.* **79**, 5870–5876.
- SHELDRIK, G. M. (1978). *SHELX*. In *Computing in Crystallography*, edited by H. SCHENK, R. OLTJOF-HAZEKAMP, H. VAN KONINGSVELD & G. C. BASSI, pp. 34–42. Delft Univ. Press.
- STEWART, R. F., DAVIDSON, E. R. & SIMPSON, W. T. (1965). *J. Am. Phys.* **42**, 3175–3187.
- VALACH, F., SIVY, P. & KOREN, B. (1984). *Acta Cryst.* **C40**, 957–959.

*Acta Cryst.* (1990). **B46**, 361–370

## An Experimental Electron Density Study of NaHC<sub>2</sub>O<sub>4</sub>·H<sub>2</sub>O at 120 K\*

BY ROBERT G. DELAPLANE, ROLAND TELLGREN AND IVAR OLOVSSON

*Institute of Chemistry, University of Uppsala, Box 531, S-751 21 Uppsala, Sweden*

(Received 18 November 1988; accepted 3 January 1990)

### Abstract

Sodium hydrogen oxalate monohydrate,  $M_r = 130.03$ , triclinic,  $P\bar{1}$ ,  $a = 6.4235$  (7),  $b = 6.6580$  (8),  $c = 5.6941$  (10) Å,  $\alpha = 85.048$  (9),  $\beta = 110.100$  (13),  $\gamma = 104.963$  (14)°,  $V = 220.94$  Å<sup>3</sup>,  $Z = 2$ ,  $D_x = 1.954$  Mg m<sup>-3</sup>,  $\lambda(\text{Mo } K\alpha) = 0.71069$  Å,  $\mu = 0.293$  mm<sup>-1</sup>,  $F(000) = 132$ ,  $T = 120$  K,  $R = 0.0279$  for conventional refinement based on 3971 reflections with  $F_o^2 > 3\sigma(F^2)$ . The deformation electron density of NaHC<sub>2</sub>O<sub>4</sub>·H<sub>2</sub>O has been measured at 120 K using X-ray and neutron diffraction techniques.  $X$ - $X$  (high order) and  $X$ - $N$  difference density maps are compared with deformation maps derived from a multipole model. Deformation densities in the covalent bonds of the HC<sub>2</sub>O<sub>4</sub><sup>-</sup> ion are correlated with bond order. Deformation densities in the three independent hydrogen bonds are consistent with an electrostatic model for bonds of weak to intermediate strength in which polarization and other contributions become more important as the proton-acceptor distance decreases. The hydrogen bonding affects both the covalent bonds and the lone-pair electron density of the acceptor oxygen atoms.

### Introduction

The effect of the crystalline field on the charge density of the water molecule has been the subject of a series of investigations at this institute (*cf.* Hermansson, 1984, and references therein). Studies of the electron density in solids by diffraction tech-

niques include numerous examples containing hydrogen bonds (Olovsson, 1980); however, the number of accurate low-temperature investigations remains limited. The extensive electron density studies of oxalic acid dihydrate (Coppens *et al.*, 1984) permit detailed comparison with the corresponding density distribution in the hydrogen oxalate ion. In addition to both single and double C—O bonds, the HC<sub>2</sub>O<sub>4</sub><sup>-</sup> ion contains two intermediate C—O bonds with the oxygen atoms in rather different environments.

The crystal structure and deformation electron density of NaHC<sub>2</sub>O<sub>4</sub>·H<sub>2</sub>O have been investigated previously at 295 K using X-ray and neutron diffraction (Tellgren, Thomas & Olovsson, 1977). The electron density of the H<sub>2</sub>O molecule and HC<sub>2</sub>O<sub>4</sub><sup>-</sup> ion including the crystal field effects in NaHC<sub>2</sub>O<sub>4</sub>·H<sub>2</sub>O was studied theoretically using *ab initio* MO-LCAO-SCF calculations by Lunell (1984). We present here an experimental study of the charge density distribution in NaHC<sub>2</sub>O<sub>4</sub>·H<sub>2</sub>O at 120 K using three different procedures for calculating dynamic deformation density maps:  $X$ - $N$  difference densities,  $X$ - $X$  (high-order) refinements and multipole model refinements. Details of the neutron diffraction study at 120 K have previously been reported (Delaplane, Tellgren & Olovsson, 1984).

### Experimental

#### Data collection and reduction

Crystals of sodium hydrogen oxalate monohydrate were grown by slow evaporation of an aqueous solution. The crystal selected for data collection was

\* Hydrogen Bond Studies. 155. Part 154: Fernandes, Tellgren & Olovsson (1988).

an elongated prism of dimensions  $0.07 \times 0.21 \times 0.08$  mm for the  $\{100\}$ ,  $\{010\}$  and  $\{001\}$  forms, respectively. The specimen was mounted in an arbitrary orientation on an Enraf-Nonius CAD-4 automatic diffractometer, and cooled by a stream of cold nitrogen gas on a locally constructed low-temperature device. The temperature was 120 (2) K as measured by a microthermocouple. Cell dimensions were determined by a least-squares refinement for the Mo  $K\alpha_1$  peaks of 32 reflections for which  $2\theta > 60^\circ$ .

Intensities were measured with graphite-monochromated Mo  $K\alpha$  radiation ( $\lambda = 0.71069 \text{ \AA}$ ) using an  $\omega/2\theta$  step-scan. Five monitor reflections were remeasured every 3 h to check the stability of the crystal and temperature. All 6886 reflections with  $\sin\theta/\lambda \leq 0.96 \text{ \AA}^{-1}$  were measured. Intensities for reflections in the range  $0.96 < \sin\theta/\lambda < 1.32 \text{ \AA}^{-1}$  were predicted from a structure-factor calculation using atomic parameters from a preliminary least-squares refinement; only those predicted to have an intensity larger than twice background were measured. The additional 3615 reflections in this range gave a total of 10 501 measurements. The five monitor reflections decreased in intensity by 8% during the 45 days of data collection. A 2% decrease was noted during the first 20 days, when reflections with  $\sin\theta/\lambda \leq 0.87 \text{ \AA}^{-1}$  were measured. At higher angles variations in the monitored intensities were more pronounced, due in part to the formation of ice which was removed periodically from the crystal. 411 reflections with  $\sin\theta/\lambda \leq 0.60 \text{ \AA}^{-1}$  were remeasured at the end of the data collection. After rescaling there were no significant differences from measurements at the beginning of data collection indicating that there was no detectable change in extinction.

Intensities were corrected for background radiation using the profile-analysis method of Lehmann & Larsen (1974). The data were rescaled from the variations of the monitor intensities during data collection, following the procedure of McCandlish, Stout & Andrews (1975). Variances for the intensities were estimated from counting statistics and the scatter of the monitors. The intensities were corrected for Lorentz-polarization and for absorption, utilizing Gaussian quadratures with a  $4 \times 8 \times 4$  grid. The transmission factors ranged from 0.961 to 0.983. The agreement among symmetry-related reflections was compared with that expected for a normal distribution using a normal probability plot of  $\delta R = (F_o^2 - \bar{F}_o^2)/\sigma_c(\bar{F}_o^2)$  (Abrahams & Keve, 1971; Lundgren & Liminga, 1979).  $\bar{F}_o^2$  is the average of the equivalent reflections *i.e.* Friedel pairs for the triclinic system;  $\sigma_c(\bar{F}_o^2)$  was derived from counting statistics. The plot was linear with a slope of 0.73 and  $y$  intercept of 0.06, indicating an overestimation of the e.s.d.'s by a factor of 1.37. During data collection, members of

Table 1. Summary of least-squares refinements

	A	B	B*	C	C*
	Conventional	High-order		Deformation	
$\sin\theta/\lambda$ range ( $\text{\AA}^{-1}$ )	0.0-1.35	0.85-1.10		0.0-1.35	
No. of reflections, $m$	3971	1407	1407	3971	3971
No. of variables, $n$	85	73	49	231	207
Scale factor (multiplies $F_o$ )	0.2526	0.2538	0.2540	0.2509	0.2511
$R(F^2) = \sum   \Delta   / \sum F_o^2$ where $\Delta = (F_o^2 - k^2 F_c^2)$	0.0387	0.0502	0.0519	0.0280	0.0286
$wR(F^2) = (\sum w \Delta^2 / \sum w F_o^4)^{1/2}$	0.0674	0.0631	0.0651	0.0371	0.0379
$R(F) = \sum   F_o - k F_c   / \sum F_o$	0.0279	0.0331	0.0342	0.0218	0.0222
$S(F^2) = [\sum w \Delta^2 / (m - n)]^{1/2}$	1.653	1.103	1.128	1.199	1.219
No. of reflections with $ \Delta/\sigma  > 3.0$	204	7	6	41	41
Maximum $ \Delta/\sigma $	11.9	3.6	3.8	6.1	6.8
$\delta R$ plot					
Slope	0.72	0.93	0.91	0.87	0.85
$y$ intercept	-0.06	-0.09	-0.09	-0.04	-0.05
No. of reflections out of the range $-4 < \delta R < 4$	102	0	0	9	12

\* Atomic coordinates not refined (see text).

each Friedel pair were measured consecutively and once only; thus the plot does not include inaccuracies in corrections for monitor intensity variations and may underestimate errors due to the instability of the instrument and crystal. For these reasons the  $\sigma_c(\bar{F}_o^2)$  values were not modified. Equivalent intensities were averaged, providing 4972 intensities for the least-squares refinements; the agreement index for averaging,  $R_{\text{int}} = \sum (F_o^2 - \bar{F}_o^2) / \sum \bar{F}_o^2$ , was 0.024.

### Structure refinements

Three different refinement procedures were used: (A) conventional free-atom refinement with all data; (B) high-order free-atom refinement including only reflections within the interval  $0.85 < \sin\theta/\lambda < 1.10 \text{ \AA}^{-1}$ ; (C) multipole deformation refinement using the model proposed by Hirshfeld (1977). Computer programs for the data processing and refinements are described by Lundgren (1982). The full-matrix least-squares refinements minimized the function  $w(F_o^2 - k^2 F_c^2)^2$  where  $w^{-1} = \sigma_c^2(F_o^2) + (0.02 F_o^2)^2$ . Reflections with  $F_o^2 < 3\sigma(F_o^2)$  were treated as unobserved and were excluded. Spherical-atom scattering factors and anomalous-dispersion corrections were taken from *International Tables for X-ray Crystallography* (1974). Additional details are summarized in Table 1.

(a) The variables for conventional refinement A were an overall scale factor, positional and anisotropic displacement parameters for non-hydrogen atoms and positional and isotropic displacement parameters for hydrogen atoms. An isotropic secondary-extinction parameter (Becker & Coppens, 1974, 1975) refined to an insignificant value; consequently, no extinction correction was applied in subsequent refinements.

(b) High-order refinement B included only 1407 reflections with  $0.85 < \sin\theta/\lambda < 1.10 \text{ \AA}^{-1}$ . This procedure excludes the reflections most affected by bonding and lone-pair electron density. As the

cut-off value of  $\sin\theta/\lambda$  is increased, the intensities become weaker and the background contribution from thermal diffuse scattering increases. The risk of truncation errors also increases (Denne, 1977). In addition the stability of the effective temperature of the crystal for all orientation angles becomes more difficult to maintain at high  $\theta$  with the cold-stream cooling technique. For these reasons the initial high-angle refinements included reflections for several different intervals of  $\sin\theta/\lambda$ ; the choice of  $0.85 < \sin\theta/\lambda < 1.10 \text{ \AA}^{-1}$  was based on the  $R$  values and the quality of the deformation density maps calculated from the atomic parameters for each refinement. Refinement of the hydrogen-atom parameters was not possible using data in this angular range. The values for these parameters were therefore taken from neutron diffraction results (Delaplane, Tellgren & Olovsson, 1984). Because the average of the neutron displacement parameters for the non-hydrogen atoms was 6% higher than those for the high-order refinement, the displacement parameters for the hydrogen atoms were divided by a scale factor of 1.057. In the final refinement the hydrogen-atom parameters were fixed; positional and anisotropic displacement parameters for the non-hydrogen atoms and the scale factor were varied. A comparison of the positional parameters with those from the neutron data suggested that the high-angle refinement was still slightly affected by bonding electron density. In a modified refinement  $B'$ , identical to  $B$  except that the positional parameters for all atoms were held constant at the neutron values, only thermal parameters for the non-H atoms and a scale factor were refined.

(c) The multipole deformation density refinements  $C$  are based on an expansion of deformation functions which allows for deviations from the spherical free-atom densities due to bonding. In the model described by Hirshfeld, the total static density is represented as a superposition of free-atom densities plus a linear combination of local atomic deformation functions centered at each atomic site. For each atom  $\rho = \rho_a^{\text{at}} + \sum_n C_{a,n} \rho_{a,n}$ , where the coefficients  $C_{a,n}$  are varied in the refinement. Each atomic deformation function has the form  $\rho_{a,n} = N_n r^n e^{-\alpha r} \cos^n \theta_k$ , where the factor  $N_n$  normalizes the density factor,  $r$  is the distance from the atomic nucleus,  $\theta_k$  is the angle between  $r$  and a specified polar axis  $k$ , and  $n$  is an integer between zero and four. The adjustable parameter  $\alpha$  determines the radial distribution for each set of functions. Alternatively the exponential factor  $e^{-\alpha r}$  may be replaced by the Gaussian function  $e^{-\gamma r^2}$ . A maximum of 35 functions is possible for each atom, but the use of local (chemical) symmetry greatly reduces this number.

In order to study the effect of hydrogen bonding on the deformation density, a minimum of local

symmetry was imposed. The oxalate fragment was assumed to be planar, and the constituent carbon and oxygen atoms constrained to have local  $m$  symmetry with respect to this plane.  $\text{Na}^+$  was restricted to octahedral symmetry, while hydrogen atoms were assigned cylindrical symmetry about the O—H bonds. The local symmetry assigned to the water molecule ( $m$ ) was defined with respect to the plane bisecting the angle H(1)—O( $W$ )—H(2) and perpendicular to the water plane; thus H(1) and H(2) have identical deformation functions. In all multipole models as in the high-order refinements the positional and displacement parameters for the hydrogen atoms were constrained to their neutron diffraction values.

As the convergence of earlier refinements with exponential radial functions  $e^{-\alpha r}$  was often difficult (Legros & Kvick, 1980; Hermansson & Thomas, 1982), Gaussian radial functions were used initially, the exponents  $\gamma$  being assigned constant values of  $3.5 \text{ \AA}^{-2}$  (Lundgren, 1979). Deformation functions up to the octapole level ( $n \leq 3$ ) were assigned to the non-hydrogen atoms but were limited to the quadrupole level ( $n \leq 2$ ) for hydrogen atoms. Positional and anisotropic displacement parameters for non-hydrogen atoms, 118 deformation coefficients and a scale factor were varied. The refinement converged without difficulty, but resulting deformation density maps contained charge density features ranging up to  $0.40 e \text{ \AA}^{-3}$  in height at the atomic centers. The deformation parameters were correlated with the scale factor and displacement parameters in such a way that part of the free-atom density had been replaced by multipole density.

The Gaussian radial functions were then replaced by the less compact exponential functions  $e^{-\alpha r}$ . To improve flexibility, the set of functions on  $\text{Na}^+$ , C and O was extended to hexadecapole level ( $n = 4$ ). The local symmetry constraints were unchanged. Additional refinements followed the guidelines given by Hirshfeld (1971). The coefficients  $\alpha$  were assigned fixed values of 6.0, 5.5, 6.0 and  $4.0 \text{ \AA}^{-1}$  for Na, C, O and H, respectively. The initial scale factor and atomic parameters, obtained from the high-order refinement  $B$ , were not varied in the early cycles. For the final cycles, 231 parameters, of which 158 were deformation function coefficients, were refined. Because the variation of  $\langle w|\Delta F^2| \rangle$  as a function of  $F_o^2$  and  $\sin\theta/\lambda$  indicated poor agreement for several intense reflections at low angles, the weighting scheme was modified to  $w^{-1} = \sigma^2 [F_o^2 + (0.005 F_o^2/S)]^2$  where  $S = \sin\theta/\lambda$ . Refinement of the exponential coefficients  $\alpha$  failed because of correlation with the other parameters. Refinements with  $\alpha$  modified by  $\pm 0.5 \text{ \AA}^{-1}$  did not affect the  $R$  values significantly although changes were noted in the deformation coefficients. The insensitivity of the agreement fac-

tors for small variations in  $\alpha$  was noted by Hirshfeld (1971) who pointed out that the set of deformation parameters is redundant because it enables the same density to be defined by different sets of values for the coefficients. Finally, an additional refinement  $C'$  with the positional parameters for all atoms fixed to the neutron values was carried out. The procedure differs from a joint ( $X + N$ ) refinement of a multipole model where all parameters simultaneously fit both X-ray and neutron data (Coppens, Boehme, Price & Stevens, 1981). In the following discussion it will be referred to as an ( $X, N$ ) multipole refinement.

## Results and discussion

### Comparison of different refinements

The crystal structure is illustrated in Fig. 1 using the parameters from the neutron refinement. The hydrogen oxalate ions are linked lengthwise by hydrogen bonds [ $2.567(1) \text{ \AA}$ ] to form infinite chains in the  $c$  direction which are joined crosswise *via* hydrogen-bonded water molecules and electrostatic interactions with  $\text{Na}^+$  ions. The structure at 295 K has previously been described (Tellgren & Olovsson, 1971; Tellgren, Thomas & Olovsson, 1977). The largest structural changes caused by reducing the temperature from 295 to 120 K are contractions of the  $\text{O}\cdots\text{O}$  hydrogen-bond distances varying from 0.005 to 0.018  $\text{\AA}$ ; decreases in the  $\text{Na}^+\cdots\text{O}$  distances range from 0.006 to 0.022  $\text{\AA}$ .

The results for the five refinements, summarized in Table 1, show that the model including deformation functions gives significantly better agreement with the observed structure factors than the conventional spherical free-atom model.\* Differences between the scale factors for the various refinements are less than 1%. Residual density maps for the the conventional refinement showed peaks up to  $0.35 \text{ e \AA}^{-3}$  in the C—C and all four C—O bonds whereas residual maps for the deformation model were nearly flat with a maximum density of  $0.15 \text{ e \AA}^{-3}$ . The positional parameters for the different refinements are compared with those from a neutron diffraction study at 120 K (Delaplane, Tellgren & Olovsson, 1984) in Table 2. Interatomic distances and angles are given in Table 3.

As expected the O—H distances from the conventional X-ray refinement are about 0.1  $\text{\AA}$  shorter than the neutron values. For the non-hydrogen atoms, the positional parameters from the high-order and multi-

pole refinements agree well; the maximum difference is  $1.5\sigma$ , where  $\sigma$  is the combined standard deviation. The C—O distances for the multipole model are only slightly shorter (0.001  $\text{\AA}$ ) indicating that these oxygen positions are little affected by lone-pair density. The largest discrepancy between the conventional and the latter two refinements is  $3.7\sigma$  for the  $y$  coordinate of O(1) which contributes to a total displacement of 0.003  $\text{\AA}$  towards the lone-pair region for this atom. Similar shifts, averaging 0.001  $\text{\AA}$  for the three remaining oxygen atoms in the  $\text{HC}_2\text{O}_4^-$  ion and 0.002  $\text{\AA}$  for O( $W$ ), are directed away from the hydrogen atoms. For O( $W$ ) this aspherical shift with respect to the neutron diffraction results is 0.005  $\text{\AA}$  for the conventional refinement, decreasing to 0.003  $\text{\AA}$  for the high-order and multipole refinements. The remaining positional parameters for these latter two refinements agree well with the neutron parameters.

The displacement parameters\* for the high-order refinement agree well with those for the multipole model; the agreement with the conventional refinement is poorer as expected since these parameters are influenced more by bonding. The neutron displacement parameters are systematically higher than the X-ray values as mentioned above; the average ratio  $U_{ii,N}/U_{ii,X}$  ( $i = 1, 2, 3$ ) is 1.04 and 1.06 for the multipole and high-order refinements, respectively. Such inconsistencies between X-ray and neutron diffraction results occur frequently and may be due to extinction, crystal misalignment, different effective temperatures or uncorrected TDS contributions.

The validity of the displacement parameters from each refinement was examined using the rigid-bond test (Hirshfeld, 1976). Mean-square amplitudes of vibrational motion along the bond for each covalently bonded heavy atom in the hydrogen oxalate ion were calculated. The values for all pairs agree

\* See deposition footnote.

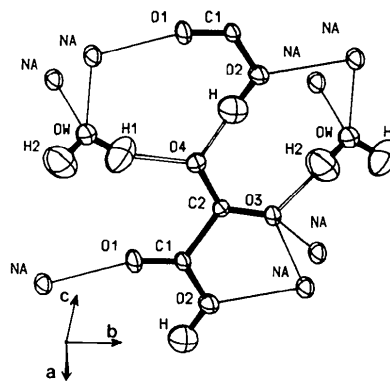


Fig. 1. The geometry of  $\text{NaHC}_2\text{O}_4 \cdot \text{H}_2\text{O}$  at 120 K. Thermal ellipsoids are plotted at 75% probability with the program ORTEP (Johnson, 1965).

\* Lists of structure factors, anisotropic thermal parameters and mean-square atomic displacements have been deposited with the British Library Document Supply Centre as Supplementary Publication No. SUP 52623 (72 pp.). Copies may be obtained through The Technical Editor, International Union of Crystallography, 5 Abbey Square, Chester CH1 2HU, England.

Table 2. Atomic coordinates ( $\times 10^5$ ;  $\times 10^4$  for H) for refinements A, B, C and N (neutron data)

		x	y	z
Na	A	25182 (4)	2704 (3)	24007 (4)
	B	25176 (8)	2712 (6)	24003 (7)
	C	25173 (2)	2712 (2)	23997 (2)
	N	25167 (22)	2705 (22)	24005 (25)
C(1)	A	25794 (7)	53920 (6)	35305 (8)
	B	25794 (11)	53917 (8)	35295 (11)
	C	25802 (4)	53920 (7)	35279 (9)
	N	25819 (12)	53938 (11)	35289 (13)
C(2)	A	27634 (7)	63965 (6)	59778 (7)
	B	27639 (11)	63962 (8)	59774 (10)
	C	27638 (5)	63966 (7)	59781 (8)
	N	27635 (11)	63980 (12)	59773 (13)
O(1)	A	24594 (6)	35479 (5)	34202 (6)
	B	24595 (12)	35502 (8)	34201 (11)
	C	24578 (4)	35513 (7)	34188 (8)
	N	24559 (15)	35496 (14)	34176 (16)
O(2)	A	26278 (7)	67291 (5)	17084 (6)
	B	26277 (12)	67276 (8)	17080 (10)
	C	26284 (4)	67267 (7)	17089 (8)
	N	26292 (15)	67270 (14)	17089 (15)
O(3)	A	33435 (6)	83356 (5)	61192 (6)
	B	33421 (10)	83344 (7)	61200 (9)
	C	33420 (4)	83330 (7)	61196 (7)
	N	33422 (14)	83344 (13)	61172 (15)
O(4)	A	23363 (6)	51414 (5)	76223 (6)
	B	23354 (12)	51424 (8)	76189 (10)
	C	23374 (5)	51424 (7)	76199 (8)
	N	23384 (15)	51455 (14)	76208 (15)
O(W)	A	14508 (7)	8222 (5)	81434 (7)
	B	14528 (11)	8247 (8)	81421 (11)
	C	14568 (14)	8238 (4)	81429 (8)
	N	14568 (14)	8263 (14)	81412 (16)
H	A	2579 (19)	6108 (17)	239 (21)
	N	2536 (3)	6049 (3)	93 (3)
	H(1)	1934 (20)	2034 (19)	7696 (22)
H(2)	A	1903 (3)	2245 (3)	7623 (4)
	N	2010 (18)	73 (15)	7483 (18)
	N	2099 (3)	-12 (3)	7407 (4)

within 0.001 Å indicating that the parameters are physically reasonable. The agreement is clearly better for the high-order and deformation refinements in which bonding effects are minimized. The good agreement for the conventional free-atom refinement is due to the large proportion of high-order reflections in the data. However, errors due to extinction or TDS effects, for example, may affect these parameters systematically in a manner that is not amenable to detection.

#### Deformation electron densities

$X-N$  difference density maps were calculated from  $F_c$  values evaluated using the atomic parameters determined from neutron diffraction and spherical free-atom X-ray scattering factors. The scale factor was that from a refinement in which the free-atom charge density coefficients were not varied. High-order  $X-X$  and  $X-(X,N)$  difference density maps were computed by a similar procedure, with the atomic parameters from the high-order refinements B and B', respectively, used for  $F_c$ .

Dynamic multipole deformation maps were derived from an  $F_c$  synthesis calculated from the deformation functions only. For each procedure the Fourier syntheses included measured reflections with  $\sin\theta/\lambda \leq 1.05 \text{ \AA}^{-1}$ ; inclusion of additional high-order

Table 3. Bond lengths (Å) and angles ( $^\circ$ )

	A	B	C	Neutron
	Conventional	High-order*	Multipole*	
C(1)—C(2)	1.553 (1)	1.553 (1)	1.554 (1)	1.554 (1)
C(1)—O(1)	1.216 (1)	1.214 (1)	1.213 (1)	1.215 (1)
C(1)—O(2)	1.311 (1)	1.310 (1)	1.309 (1)	1.308 (1)
C(2)—O(3)	1.249 (1)	1.249 (1)	1.248 (1)	1.248 (1)
C(2)—O(4)	1.254 (1)	1.253 (1)	1.253 (1)	1.253 (1)
O(2)—H	0.953 (12)	1.036 (2)	1.036 (2)	1.036 (2)
O(W)—H(1)	0.838 (12)	0.967 (2)	0.967 (2)	0.965 (2)
O(W)—H(2)	0.858 (11)	0.968 (2)	0.968 (2)	0.967 (2)
H...O(4)	1.616 (12)	1.532 (2)	1.532 (2)	1.531 (2)
H(1)...O(4)	2.017 (12)	1.877 (2)	1.877 (2)	1.879 (2)
H(2)...O(3)	1.950 (11)	1.839 (2)	1.840 (2)	1.840 (2)
O(2)...O(4)	2.567 (1)	2.568 (1)	2.567 (1)	2.566 (1)
O(W)...O(4)	2.794 (6)	2.793 (1)	2.794 (1)	2.794 (1)
O(W)...O(3')	2.807 (1)	2.807 (1)	2.807 (1)	2.806 (1)
Na...O(W)	2.305 (1)	2.306 (1)	2.305 (1)	2.307 (2)
...O(1)	2.319 (1)	2.320 (1)	2.321 (1)	2.320 (2)
...O(3)	2.352 (1)	2.354 (1)	2.354 (1)	2.352 (2)
...O(W')	2.380 (1)	2.381 (1)	2.381 (1)	2.383 (2)
...O(2)	2.446 (1)	2.448 (1)	2.449 (1)	2.449 (2)
...O(3')	2.441 (1)	2.442 (1)	2.443 (1)	2.443 (2)
O(1)—C(1)—O(2)	125.45 (4)	125.45 (6)	125.49 (6)	125.42 (8)
O(3)—C(2)—O(4)	127.21 (4)	127.16 (6)	127.21 (6)	127.19 (8)
Dihedral twist	13.03 (2)	13.01 (4)	12.96 (2)	12.90 (5)
about C(1)—C(2)				
H(1)—O(W)—H(2)	103.9 (10)	107.3 (2)	107.3 (2)	107.5 (2)
O(2)—H...O(4')	175.5 (10)	176.7 (2)	176.8 (2)	176.8 (2)
O(W)—H(1)...O(4)	154.1 (12)	157.1 (2)	157.2 (2)	157.2 (2)
O(W)—H(1)...O(3)	177.6 (9)	177.8 (2)	177.7 (2)	177.9 (2)

\*Hydrogen positions from neutron diffraction.

reflections in the difference maps increased the noise level while not enhancing charge density in regions associated with bonding. The effective errors in the maps, excluding the immediate area around atom centers, are estimated at  $0.05 e \text{ \AA}^{-3}$  (Rees, 1977) from a comparison of densities in chemically equivalent regions of the maps.

#### The $\text{HC}_2\text{O}_4^-$ ion

The  $X-N$ ,  $X-(X,N)$  high-order and  $(X,N)$  multipole deformation densities in the hydrogen oxalate ion are compared in Figs. 2(a), 2(b) and 2(c), respectively. As the ion is twisted  $12.9^\circ$  about the C(1)—C(2) bond, each map is plotted separately for each end of the ion; maps for both halves are presented together as if the ion were completely planar. Well-defined concentrations of electron density occur in all of the covalent bonds and in the lone-pair regions around the oxygen atoms, the maps resembling those obtained in the room-temperature study (Tellgren, Thomas & Olovsson, 1977). The densities in the present investigation are more pronounced due to the reduced temperature and improved resolution.

The general features in all of the three maps are similar, and quantitative agreement among corresponding covalent bond densities is good. The contour lines of the multipole map are smoother as the deformation functions filter out most of the noise at the expense of not reproducing faithfully the sharp features at the lone-pair regions in the maps 2(a) and 2(b). The peak height differences of  $\leq 0.15 e \text{ \AA}^{-3}$  are especially noticeable in the O(1) and O(4) lone-pair

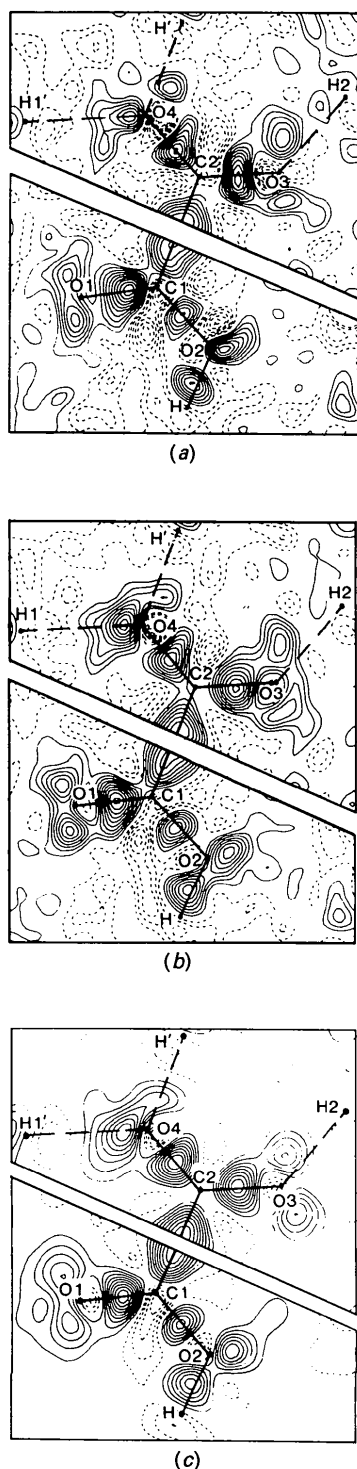


Fig. 2. Experimental deformation densities in the  $\text{HC}_2\text{O}_4^-$  ion. Each composite map has been plotted separately through the O(1), C(1), O(2) and O(3), C(2), O(4) planes. (a)  $X-N$  difference density, (b) high-order  $X-(X,N)$  difference density, (c) dynamic  $(X,N)$  multipole deformation density. Contours here and in the following figures are at intervals of  $0.05 \text{ e } \text{\AA}^{-3}$ . Solid and dashed lines denote positive and negative contours, respectively; the zero level has been omitted.

densities. Contour lines in the  $X-N$  map are more irregular than those in the  $X-(X,N)$  high-order map, which is attributed to discrepancies in the displacement parameters, with increasing errors in the density maps near the atomic nuclei (Rees, 1977). Maps from high-order and multipole models including refinement of positional parameters for non-hydrogen atoms were similar to 2(b) and 2(c), respectively. The largest differences ( $\leq 0.05 \text{ e } \text{\AA}^{-3}$ ) were the higher peaks for some of the lone-pair regions of the maps based on neutron atomic positions.

The elongation of the peak in the C(1)—C(2) bond resembles that found in the C—C bond in oxalic acid (Coppens *et al.*, 1984). The bond densities in each of the three C—O bonds are as expected from the relative bond orders. The C(1)—O(1) double bond is distinguishable from the C(1)—O(2) single bond (peak heights of  $0.50$  and  $0.30 \text{ e } \text{\AA}^{-3}$ , respectively). The shapes of densities for the intermediate C(2)—O(3) and C(2)—O(4) bonds are between those for single- and double-bond densities.

The integral of the positive bond densities in the C—C and C—O bonds was estimated numerically; negative densities were not included. Using a  $0.1 \text{ \AA}$  three-dimensional grid, boundaries between merging bonding and lone-pair regions of density were drawn through points of minimum density. This crude definition of bond deformation density must be used with caution, but the procedure is more meaningful than the more common practice of comparing heights in selected planes. The values of  $0.11$ ,  $0.08$ ,  $0.05$  and  $0.04 \text{ e}$  for C(1)—O(1), C(2)—O(3), C(2)—O(4) and C(1)—O(2), respectively, agree with the decrease of bond order from a double to a single bond. The density in C—C bonds has been correlated with bond length for a number of different molecules (Berkovitch-Yellin & Leiserowitz, 1975). The estimated C(1)—C(2) bond density of  $0.09 \text{ e}$  compares well with a value of  $0.087 \text{ e}$  predicted from the correlation for a bond length of  $1.553 \text{ \AA}$ .

Cross sections for the multipole deformation densities through the bond midpoints and perpendicular to the bond axes are shown in Fig. 3. The degree of asphericity in the cross section of each bond varies systematically. In the perpendicular cross sections, ratios between the vertical and horizontal diameters of the first contour with respect to the planes defining the ion are  $1.07$ ,  $1.20$ ,  $1.75$ ,  $1.22$  and  $1.30$  for C(1)—C(2), C(1)—O(1), C(1)—O(2), C(2)—O(3) and C(2)—O(4), respectively. The order of these values agrees with those calculated for the static deformation densities in the  $\text{HC}_2\text{O}_4^-$  ion (Lunell, 1984). The cross-section density for the C(1)—C(2) bond in the vertical direction is less elongated than that for the C—C bond in oxalic acid as determined experimentally at  $100 \text{ K}$  (Stevens & Coppens, 1980) and from theoretical studies (Johansen, 1979; Stevens,

1980). The  $\pi$  character of this bond decreases from the acid molecule to the  $\text{HC}_2\text{O}_4^-$  ion when the bond is lengthened from 1.544 (1) to 1.553 (1) Å. Surprisingly, the asphericity is greatest for the single C(1)—O(2) bond although the cross-section area is less than that for the other bonds.

There are well-developed peaks in the lone-pair regions of all the oxygen atoms (Fig. 2). However, the maxima lie close to the atomic centers, and densities within 0.3 Å of the nuclei are subject to increased error (Rees, 1977). Double maxima are found in the plane of the ion for O(1), O(3) and O(4) as expected for  $sp^2$  hybrid bonding whereas the  $sp^3$  bonded O(2) exhibits a single peak in the plane. The differences in the hydrogen-bond acceptor role of O(3) and O(4) are also evident in the lone-pair regions of these atoms: the O(3) lone-pair density in the plane of the ion appears as two lobes of similar density; for O(4) the density in the direction of the shorter hydrogen bond, O(4)⋯H—O(2), is less than that in the O(4)⋯H(1)—O(W) direction. This point is further discussed below in the section *The hydrogen bonds*.

The high-order  $X(X,N)$  difference density in cross sections normal to each C—O bond and intersecting the extended axis 0.1 Å behind each respective oxygen atom is plotted in Fig. 4. The O(2) lone-pair density is illustrated by the section which bisects the C(1)—O(2)—H angle. The double-bonded O(1) lone-pair density in Fig. 4(a) shows two well-defined maxima lying in the O(1)—C(1)—O(2) plane, consistent with those in Fig. 2. This compact density is little affected by the crystalline environment as O(1) is involved in a single interaction with  $\text{Na}^+$  which deviates only 0.18 Å from the extended O(1)—C(1)—O(2) plane. The lone-pair density of O(2) in Fig. 4(d) extends above and below the C—O—H plane in a single peak which differs distinctly from the double lobe of O(1). This difference for single- and double-bonded oxygen agrees with earlier theoretical and experimental results (*cf.* Olovsson, 1982).

An excess of deformation density appears in the double-lobe regions around O(3) and O(4) which is less concentrated in the plane of the ion than for O(1) (Fig. 2). These lone-pair features are expected

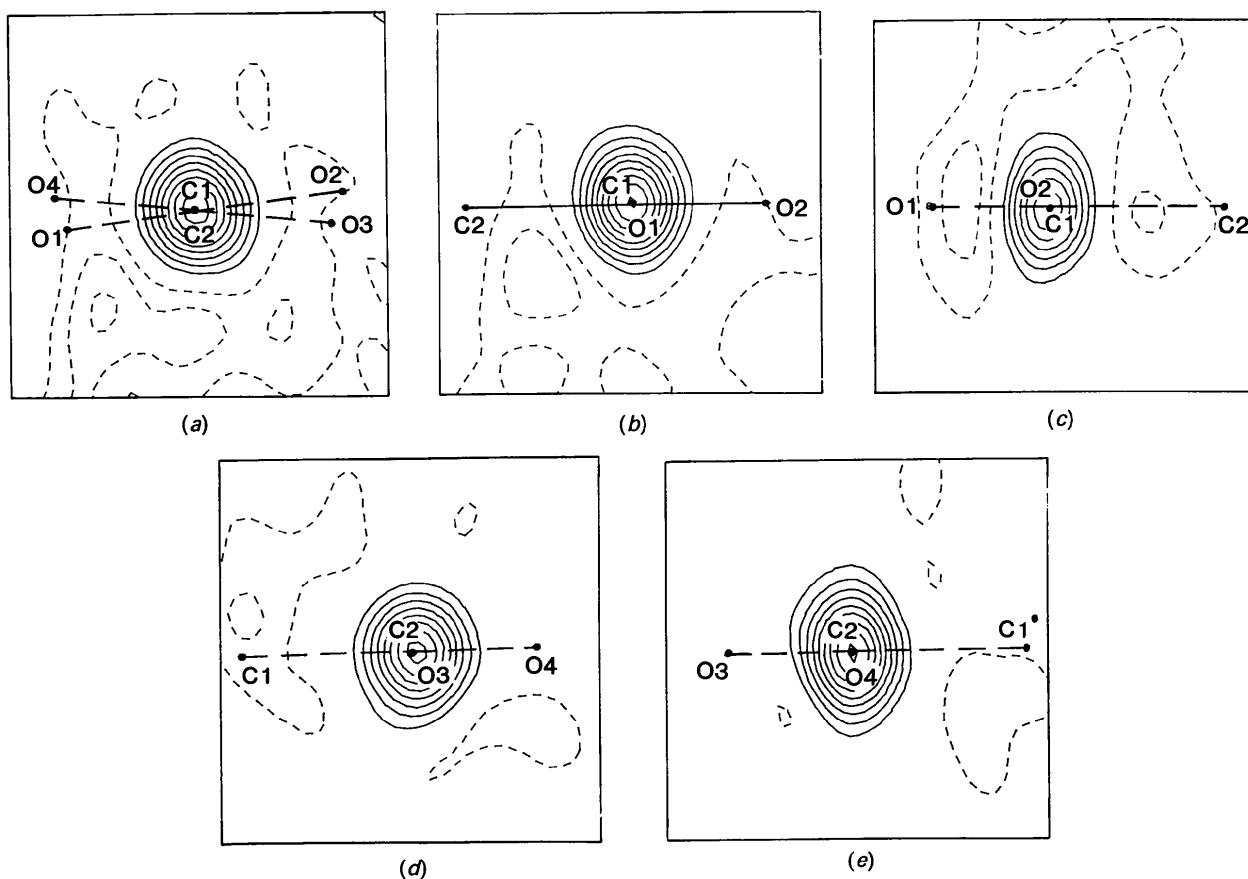


Fig. 3. Dynamic  $(X,N)$  multipole deformation density sections perpendicular to the bond axes and through their midpoints. Contours as in Fig. 2. Bonds (a) C(1)—C(2), (b) C(1)—O(1), (c) C(1)—O(2), (d) C(2)—O(3), (e) C(2)—O(4).

to have characteristics between those of O(1) and O(2). In addition, O(3) and O(4) have stronger interactions with the crystalline environment which is expected to affect their lone-pair densities more than that of O(1) and O(2). A detailed study suggests that both these factors are responsible for the characteristics of the O(3) and O(4) lone-pair densities.

### The H<sub>2</sub>O molecule

The deformation density near the water molecule is shown in Figs. 5 and 6. The water molecule forms hydrogen bonds of about equal strength with the acceptors O(3) and O(4), and the density peaks in the bonds O(W)—H(1) and O(W)—H(2) are similar, as expected. O(W) has a distorted tetrahedral environment with two O(W)⋯Na<sup>+</sup> contacts with distances of 2.307 (2) and 2.383 (2) Å. As in the free water molecule the lone-pair deformation density here appears as a single lobe which extends diffusely into the region between the two Na<sup>+</sup> ions. The distortional effect of the Na<sup>+</sup> ions on this lone-pair density is difficult to estimate in this study. Theoretical model calculations of isolated H<sub>2</sub>O⋯M<sup>n+</sup> dimers demonstrate, however, such an influence of the

cation on the electron density of the water molecule (Hermansson, Olovsson & Lunell, 1984).

### Dipole moment of the water molecule

The charge of the water molecule was first calculated by integration of the deformation density over a polyhedral volume defined by boundary planes perpendicular to vectors between the constituent atoms of the water molecule and its nearest neighboring atoms (Coppens, Moss & Hansen, 1980). The point of intersection of each boundary on a vector is determined by the ratio of the radii of each atom pair. Van der Waals radii of 1.4 and 1.2 Å were used for oxygen and hydrogen, respectively. Na<sup>+</sup> was assigned an ionic radius of 0.97 Å. Integrations were performed with the program *DEBYE* on  $F_c$  for the model deformation refinements and on  $\Delta F$  for both  $X-N$  and high-order  $X-(X,N)$  refinements. The net charge on the water molecule was found not to differ significantly from neutrality and this permitted the calculation of an origin-independent dipole moment, by a procedure similar to that followed when determining the charge. An average value of  $8.13(3) \times 10^{-30}$  C m [2.44(1) debye] was found for the total

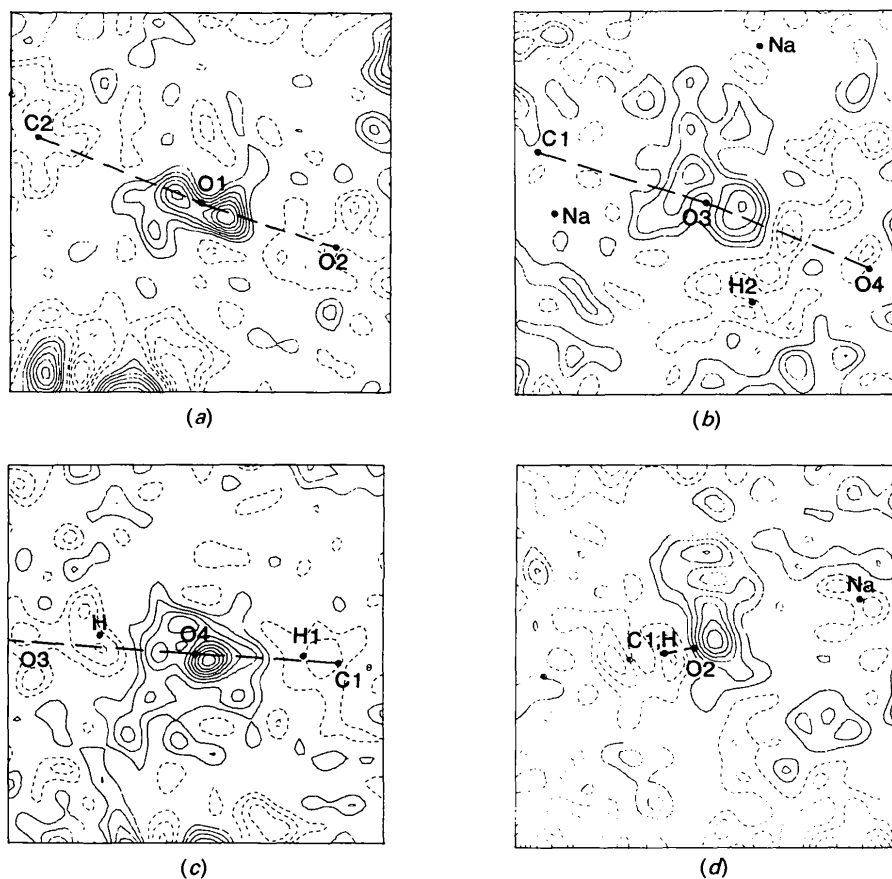


Fig. 4. High-order  $X-(X,N)$  difference density sections perpendicular to the bond axes and through a point 0.1 Å behind the oxygen atoms. Contours as in Fig. 2. (a) C(1)—O(1), (b) C(2)—O(3), (c) C(2)—O(4) bond. (d) High-order  $X-(X,N)$  difference densities in a section perpendicular to the O(1), C(1), O(2) plane through the bisector of the C(1)—O(2)—H angle. Contours as in Fig. 2.

dipole moment. The direction is defined by a vector bisecting the  $H(1)-O(W)-H(2)$  angle and lying in the molecular plane. As the water molecule lies in an approximately tetrahedral crystal field the direction of this vector would not be expected to differ signifi-

cantly from that for the free molecule. Calculations repeated for a narrow range of van der Waals radii gave similar results which indicated that the value for the dipole moment was not strongly dependent on the integration volume. Comparison with the value of  $6.16 \times 10^{-30}$  C m (1.85 debye) for the dipole moment of the free water molecule indicates an increase in dipole moment owing to interactions with the environment in the crystal. These conclusions are supported by theoretical calculations which predict a similar increase due to the crystal field in  $Na-HC_2O_4 \cdot H_2O$  (Almlöf, Lindgren & Tegenfeldt, 1972; Lunell, 1984).

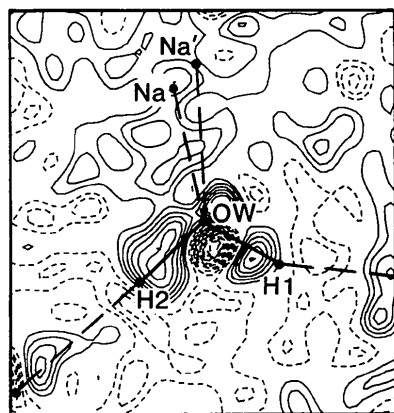
#### The $Na^+$ ion

Each  $Na^+$  ion is surrounded by six oxygen atoms to form a distorted octahedron. Deformation maps through planes including the  $Na^+$  ion are almost featureless. There is a slight excess of density ( $0.15 e \text{ \AA}^{-3}$ ) near the direction of the shortest  $Na^+ \cdots O$  contact; however, the significance of this peak is doubtful because of its proximity to the nucleus.

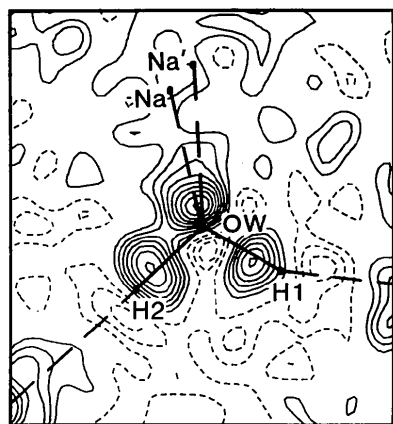
#### The hydrogen bonds

The deformation densities near the three  $O-H \cdots O$  hydrogen bonds, in Figs. 2 and 5, resemble those typical for hydrogen bonds of weak to moderate strength: an excess of charge density in the  $O-H$  bond and near the acceptor, with a slight deficiency near the proton in the acceptor direction.

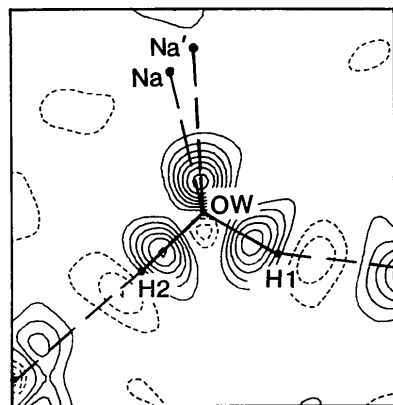
The charge distribution for hydrogen bonds of different strengths has been discussed by Olovsson (1980) and Hermansson (1985). To a first approximation, the electron density may be described as a superposition of the electron density of the isolated monomers. As a hydrogen bond is formed, these monomer polarities are increased with additional charge flow. The juxtaposition of the deficiency



(a)



(b)



(c)

Fig. 5. Deformation densities through the plane of the water molecule. (a)  $X-N$  difference density, (b) high-order  $X-(X,N)$  difference density, (c) dynamic  $(X,N)$  multipole deformation density. Contours as in Fig. 2.

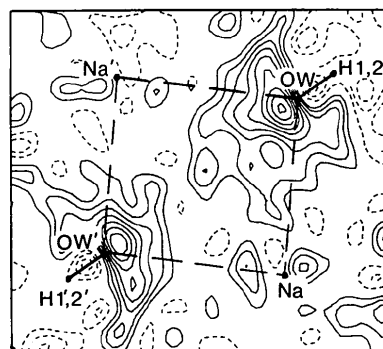


Fig. 6. Deformation density in a plane perpendicular to the water molecule and bisecting the  $H(1)-O(W)-H(2)$  angle. High-order  $X-(X,N)$  difference density. Contours as in Fig. 2.

region near H with the lone-pair density of the acceptor oxygen decreases the original lone-pair density as the O...O distance diminishes (Eisenstein & Hirshfeld, 1983; Lunell, 1984). For this reason the O(4) lone-pair density (Fig. 2) is depleted most in the direction of the shorter hydrogen bond [O...O distance = 2.566 (1) Å].

Financial support from the Swedish Natural Science Research Council is gratefully acknowledged. We are indebted to Mr H. Karlsson for assistance with the data collection. We wish to thank Professor Philip Coppens for making the computer program *DEBYE* available to us.

#### References

- ABRAHAMS, S. C. & KEVE, E. T. (1971). *Acta Cryst.* **A27**, 157–165.
- ALMLÖF, J., LINDGREN, J. & TEGENFELDT, J. (1972). *J. Mol. Struct.* **14**, 427–437.
- BECKER, P. & COPPENS, P. (1974). *Acta Cryst.* **A30**, 129–147.
- BECKER, P. & COPPENS, P. (1975). *Acta Cryst.* **A31**, 417–425.
- BERKOVITCH-YELLIN, Z. & LEISEROWITZ, L. (1975). *J. Am. Chem. Soc.* **97**, 5627–5628.
- COPPENS, P., BOEHME, R., PRICE, P. F. & STEVENS, E. D. (1981). *Acta Cryst.* **A37**, 857–863.
- COPPENS, P., DAM, J., HARKEMA, S., FEIL, D., FELD, R., LEHMANN, M. S., GODDARD, R., KRUGER, C., HELLNER, E., JOHANSEN, H., LARSEN, F. K., KOETZLE, T. F., McMULLAN, R. K., MASLEN, E. N. & STEVENS, E. D. (1984). *Acta Cryst.* **A40**, 184–195.
- COPPENS, P., MOSS, G. & HANSEN, N. K. (1980). *Computing in Crystallography*, edited by R. DIAMOND, S. RAMASESHAN & K. VENKATESAN, pp. 16.01–16.21. Bangalore: Indian Academy of Sciences.
- DELAPLANE, R. G., TELLGREN, R. & OLOVSSON, I. (1984). *Acta Cryst.* **C40**, 1800–1803.
- DENNE, W. A. (1977). *Acta Cryst.* **A33**, 438–440.
- EISENSTEIN, M. & HIRSHFELD, F. L. (1983). *Acta Cryst.* **B39**, 61–75.
- FERNANDES, N. G., TELLGREN, R. & OLOVSSON, I. (1988). *Acta Cryst.* **C44**, 1168–1172.
- HERMANSSON, K. (1984). Thesis, Univ. of Uppsala, Sweden.
- HERMANSSON, K. (1985). *Acta Cryst.* **B41**, 161–169.
- HERMANSSON, K., OLOVSSON, I. & LUNELL, S. (1984). *Theor. Chim. Acta*, **64**, 265–276.
- HERMANSSON, K. & THOMAS, J. (1982). *Acta Cryst.* **B38**, 2555–2563.
- HIRSHFELD, F. L. (1971). *Acta Cryst.* **B27**, 769–781.
- HIRSHFELD, F. L. (1976). *Acta Cryst.* **A32**, 239–244.
- HIRSHFELD, F. L. (1977). *Isr. J. Chem.* **16**, 226–229.
- International Tables for X-ray Crystallography* (1974). Vol. IV. Birmingham: Kynoch Press. (Present distributor Kluwer Academic Publishers, Dordrecht.)
- JOHANSEN, H. (1979). *Acta Cryst.* **A35**, 319–325.
- JOHNSON, C. K. (1965). *ORTEP*. Report ORNL-3794. Oak Ridge National Laboratory, Tennessee, USA.
- LEGROS, J.-P. & KVICK, Å. (1980). *Acta Cryst.* **B36**, 3052–3059.
- LEHMANN, M. S. & LARSEN, F. K. (1974). *Acta Cryst.* **A30**, 580–584.
- LUNDGREN, J.-O. (1979). *Acta Cryst.* **B35**, 1027–1033.
- LUNDGREN, J.-O. (1982). *Crystallographic Computer Programs*. Report UUIC-B13-04-05. Institute of Chemistry, Univ. of Uppsala, Sweden.
- LUNDGREN, J.-O. & LIMINGA, R. (1979). *Acta Cryst.* **B35**, 1023–1027.
- LUNELL, S. (1984). *J. Chem. Phys.* **80**, 6185–6193.
- MCCANDLISH, L. E., STOUT, G. H. & ANDREWS, L. C. (1975). *Acta Cryst.* **A31**, 245–249.
- OLOVSSON, I. (1980). *Electron and Magnetization Densities in Molecules and Crystals*, edited by P. BECKER, pp. 883–890. New York: Plenum.
- OLOVSSON, I. (1982). *Croat. Chem. Acta*, **55**, 171–190.
- REES, B. (1977). *Isr. J. Chem.* **16**, 180–186.
- STEVENS, E. D. (1980). *Acta Cryst.* **B36**, 1876–1886.
- STEVENS, E. D. & COPPENS, P. (1980). *Acta Cryst.* **B36**, 1864–1876.
- TELLGREN, R. & OLOVSSON, I. (1971). *J. Chem. Phys.* **54**, 127–134.
- TELLGREN, R., THOMAS, J. O. & OLOVSSON, I. (1977). *Acta Cryst.* **B33**, 3500–3504.

*Acta Cryst.* (1990). **B46**, 370–377

## Determination of the Crystal Structure of Recombinant Pig Myoglobin by Molecular Replacement and its Refinement

BY STEPHEN J. SMERDON, TOM J. OLDFIELD, ELEANOR J. DODSON, GUY G. DODSON,  
RODERICK E. HUBBARD AND ANTHONY J. WILKINSON\*

*Department of Chemistry, University of York, Heslington, York YO1 5DD, England*

(Received 22 August 1989; accepted 6 November 1989)

#### Abstract

As part of a protein engineering study, the X-ray crystal structure of recombinant pig myoglobin, prepared and crystallized from *E. coli*, has been determined. Diffraction data were collected to 2.5 Å

spacing using a synchrotron X-ray source. The structure was solved using the molecular-replacement method and refined using least-squares minimization procedures to a crystallographic *R* factor of 18.5% using 14 481 reflections between 10 and 2.5 Å. A preliminary comparison of the structure of pig myoglobin with other myoglobin structures is presented.

\* To whom correspondence should be addressed.